High pressure-temperature phase diagram and equation of state of titanium

Agnès Dewaele,[1] Vincent Stutzmann,[1] Johann Bouchet,[1] François Bottin,[1] Florent Occelli,[1] and Mohamed Mezouar[2]
[1]*Commissariat à l'Energie Atomique, Direction des Applications Militaires, Ile de France, 91297 Arpajon Cedex, France*
[2]*European Synchrotron Radiation Facility, BP 220, F-38043 Grenoble Cedex, France*
(Received 13 October 2014; revised manuscript received 3 February 2015; published 21 April 2015)

The high pressure-temperature behavior of titanium has been studied with x-ray diffraction in resistively heated and laser-heated diamond anvil cells up to 200 GPa and ∼3500 K. The stability fields of α-Ti, ω-Ti, β-Ti, γ-Ti, and δ-Ti have been determined in this range. γ-Ti and δ-Ti, which had been evidenced earlier under nonhydrostatic compression, are also observed in helium pressure transmitting medium. Equation-of-state parameters are proposed for α-Ti and ω-Ti at 300 K, and β-Ti at high temperature. The stability fields of the α, ω, γ, and δ phases are also studied using the projector-augmented wave method based on density-functional theory. Using the relevant core radius to avoid overlapping between atomic spheres, and relaxing cells and atomic positions, we show that all those phases have a stability domain at 0 K. We explain why γ-Ti and δ-Ti were calculated to be unstable in earlier works. In addition, a new phase, called δ'-Ti, which is a distortion of δ-Ti, is predicted to form between 80 and 120 GPa and below ≃200 K.

DOI: 10.1103/PhysRevB.91.134108 PACS number(s): 61.50.Ks, 64.30.−t, 65.40.De

I. INTRODUCTION

Titanium is of major technological interest because of its high strength, light weight, and corrosion resistance. Its performances can be further improved by controlling crystallographic phases by alloying and/or high-pressure work. Such material design, potentially guided by *ab initio* predictions, requires an accurate knowledge of the phase diagram of pure elemental titanium. At moderate pressure, titanium has a phase diagram similar to other group IV transition metals (Zr, Hf). Under ambient conditions, they crystallize in a hexagonal close-packed (hcp) structure called α. On temperature increase at ambient pressure, they undergo a phase transition to a body-centered cubic (bcc) structure labeled β below their melting temperature. They transform to the so-called ω structure (space group $P6/mmm$, Pearson symbol hP3) on pressure increase at ambient temperature. The ω structure has a hexagonal lattice; its packing is close to the bcc one, with $(0001)_\omega$ planes corresponding to the $(111)_{bcc}$ planes. Zirconium and hafnium adopt a bcc structure, above 30 and 71 GPa, respectively [1]. The sequence of phase transformations undergone by titanium is more complex and is represented in Fig. 1. At 300 K, α-Ti transforms to ω-Ti between 2 and 12 GPa, depending on the pressurizing conditions [2]. A transformation of ω-Ti to a distorded hcp structure, called γ-Ti, has been observed in diamond anvil cell experiments around 116–128 GPa [3,4]. γ-Ti has an orthorhombic lattice ($Cmcm$ space group, Pearson symbol oC4). Another polymorph called δ-Ti was observed above 140 GPa; a Rietvelt refinement of x-ray diffraction (XRD) patterns allowed proposing an orthorhombic structure close to bcc for this crystal ($Cmcm$ space group, Pearson symbol oC4) [4]. Another orthorhombic structure called η-Ti has been reported to form by thermal treatment around 80 GPa [5], and a bcc β'-Ti has been observed between 40 and 80 GPa in the same study [5].

Early density-functional theory (DFT) calculations failed in reproducing the experimental cold-compression sequence: enthalpy calculations at 0 K predicted a direct transformation of ω-Ti to bcc-Ti below 100 GPa [5,7,8]. Now, recent DFT calculations agree that γ-Ti is a stable polymorph [9–12], but the existence of δ-Ti is still debated [9–13]. A bcc phase, which we also call β-Ti in this article, is predicted to be stable above 107–162 GPa at 0 K [9–13] but has not been observed up to 220 GPa [4]. It has, therefore, been proposed that the nonhydrostatic pressurizing conditions in diamond anvil cell experiments suppresses the transformation of δ-Ti to a more symmetric phase [9,11,13,14]. Since there is no consensus on the stability of γ-Ti, δ-Ti, and η-Ti, these phases have not been included in multiphase models of titanium [6,15].

We present here an experimental and theoretical study of titanium up to 200 GPa and 3000 K, performed using XRD coupled with diamond anvil cells and DFT calculations. Helium pressure transmitting medium has been used in several experimental runs, which drastically reduced the nonhydrostatic stress on the sample [16] (this medium is often called "quasihydrostatic"). This prevents the observation of phase transitions induced by uniaxial pressurizing conditions [17]. Laser annealing was used to relax uniaxial stress and overcome possible kinetic barriers of phase transitions and reach the equilibrium. These two techniques have been used in this study to place the experimental phase diagram of titanium on a firm footing. The measurements are presented and discussed in Sec. II. DFT calculations show that the enthalpies of the different solid phases are close and, therefore, the predicted stability domains are very sensitive to calculation parameters, such as core radius and relaxation effects. Results (stability domains, lattice parameters) are put in perspective with recent predictions [9,11,13,14] and confronted to measurements in Sec. III. To finish, the experimental equation of state (EoS) of titanium at 300 K and at high temperature is presented in Sec. IV and compared to theoretical predictions and models.

II. MEASURED STABILITY FIELDS FOR HIGH PRESSURE PHASES

A. Experimental methods

Seven titanium samples have been loaded in diamond anvil cells with pressure transmitting medium and pressure gauges specified in Table I. Rhenium gaskets have been used. The

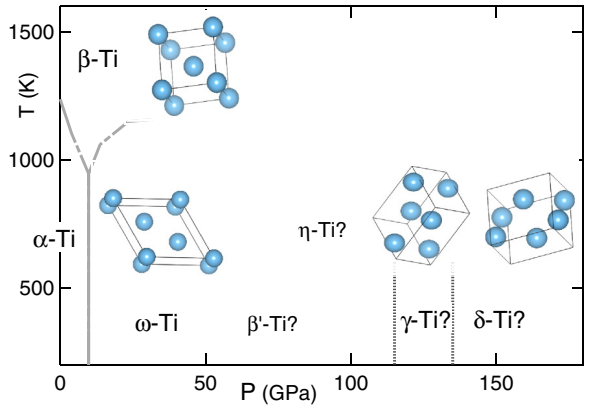

FIG. 1. (Color online) Tentative phase diagram of titanium showing the solid phases reported under high pressure. The gray lines are from Ref. [6]. The stability domains of γ-Ti and δ-Ti are from Refs. [3] and [4]. The crystal structure unit cells of β-Ti, ω-Ti, γ-Ti, and δ-Ti are represented.

first three runs in Table I aimed at a precise measurement of phase transformations and equation of state (EoS) of titanium at 300 K in helium pressure-transmitting medium [16]. For run 4, we used neon pressure medium and resistive heating to accurately locate the α-ω phase boundary. In run 1, a grain of Ti was taken from a Ti ingot with a file. For runs 2 to 4, one individual grain of titanium powder (Alfa Aesar, 99.9% purity) was loaded together with the pressure gauge in helium or neon. The thickness of the sample chamber was always larger than the dimension of the Ti grain and pressure gauge. The last four loadings were prepared for laser heating runs; for this purpose, grains of titanium (Alfa Aesar, 99.9% purity) were transformed into thin discs by compressing them between two diamond anvils. They were loaded between plates of NaCl or KCl, which allow thermal and chemical insulation of the sample from the diamond anvils during laser-heating. In run 6, an additional disk of MgO powder was placed in contact with titanium for pressure calibration purpose.

XRD diffraction experiments have been performed at the ID27 and ID09 beamlines at the European Synchrotron Radiation Facility. Monochromatic x-rays of $\simeq$0.4 Å wavelength were focused down to a 2 $\times$ 3-μm spot size, scattered off the sample, and collected on a MAR-CCD or MARE bidimensionnal detector. Resistive-heating (run 4) was performed up to 740 K by inserting the diamond-anvil cell in a ring heater. Laser heating (runs 5–7) was performed simultaneously with diffraction data collection, using two yttrium aluminum garnet (YAG) lasers with a typical total power of 10 to 100 W. XRD collection times were 20 s for the ambient temperature measurements, during which the diamond anvil cell was rotated by $\pm 8^\circ$ to $\pm 10^\circ$ and a few seconds during laser heating. The laser heating spot size was adapted to the sample size by focusing (size $\simeq 5\,\mu$m) or defocusing (size $\simeq 25\,\mu$m) the lasers. The temperature was determined from spectral radiometry measurements of the pyrometric signal from an area of 2 $\times$ 2 μm in the center of the heating spot, with an average uncertainty of 100 K. The setup and methods are described elsewhere [22,23].

TABLE I. Conditions of each experimental run. PTM: pressure-transmitting medium.

Run	P range (GPa)	T range (K)	PTM	P gauge
1	0–36	300	He	Ruby [18]
2	49–109	300	He	Ruby [18]
3	1–139	300	He	W[19]
4	1–15	444–740	Ne	SrB_4O_7
5	1–15	300–2100	NaCl	NaCl[20]
6	30–75	300–3500	KCl	KCl[21]+MgO[18]
7	50–150	300–4000	KCl	KCl[21]
8	130–200	300–3000	KCl	KCl [21]

B. Below 10 GPa: α-Ti, ω-Ti, and β-Ti

The location of the α-Ti/ω-Ti phase boundary has been studied in runs 1, 4, and 5. The α-Ti $\rightarrow$ ω-Ti phase transformation takes place between 10.1 and 14.6 GPa at 300 K in helium pressure medium, similarly to argon pressure medium [2]. This transformation has a large hysteresis: ω-Ti could be metastably preserved down to ambient pressure at 300 and 444 K. It is diminished at 737 K: the forward (reverse) transformation completed at 8.8 (1) GPa. The α-Ti/ω-Ti transition pressure P_t is evaluated as: $P_t = (P_{\rm up} + P_{\rm down})/2$, where $P_{\rm up}$ and $P_{\rm down}$ correspond to the 50% completion of α-Ti $\rightarrow$ ω-Ti and ω-Ti $\rightarrow$ α-Ti transformation, respectively. $P_{\rm up}$, $P_{\rm down}$, and P_t are plotted in Fig. 2 together with the α-ω-β triple point measured in large volume press experiments: 8.0 GPa and

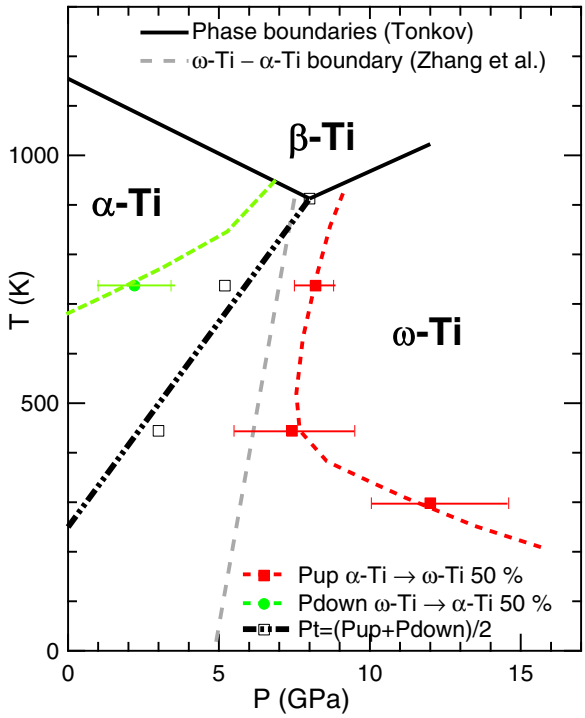

FIG. 2. (Color online) Phase boundaries between α-Ti, β-Ti, and ω-Ti according to the literature [1,24] and the present study performed under hydrostatic pressurizing conditions (runs 1 and 4). The horizontal bars represent the domain of coexistence of α-Ti and ω-Ti. The phase boundary (black dashed-double dotted line) is based on the current measurements and the triple point location [1].

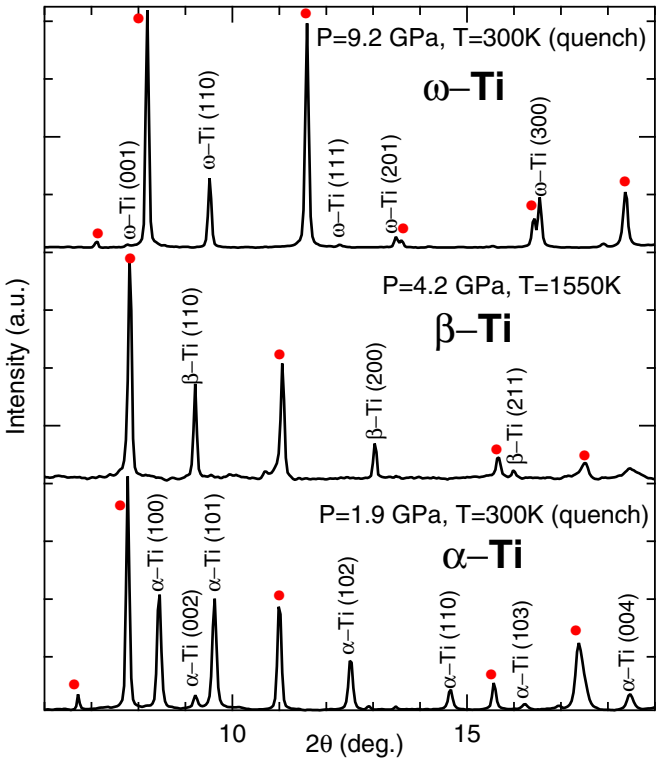

FIG. 3. (Color online) XRD patterns of α-Ti, β-Ti, and ω-Ti recorded during run 5. NaCl (pressure medium) diffraction lines are marked with red dots.

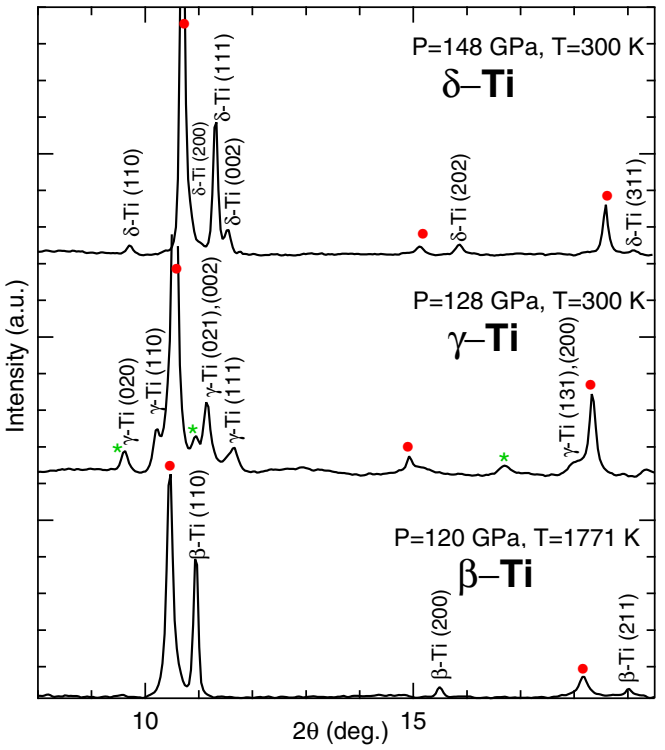

FIG. 4. (Color online) XRD patterns of β-Ti, γ-Ti, and δ-Ti recorded during run 7. KCl (pressure medium) diffraction lines are marked with red dots and rhenium gasket diffraction lines are marked with green asterisks.

913 K [1] (we assumed that this high temperature measurement is not affected by nonhydrostatic stresses or kinetic effects). The merging of this triple point with the current estimates of P_t suggest that is the ω phase, which is the stable polymorph of Ti at 0 K and 0 GPa (see Fig. 2). This confirms recent Raman spectroscopy data, which suggest that ω-Ti appears when α-Ti is cooled down below 100 K at ambient pressure [25]. We note that in establishing the α-ω transition line in Ti, the transition pressure of the direct transition alone was taken into account in some studies [24], leading to an overestimate of the transition pressure.

The current measurements are in line with previous *ab initio* results, which predict that α-Ti $\rightarrow$ ω-Ti transformation takes place around -2 GPa [9,11,14] at 0 K.

The laser-heating measurements of run 5 confirm the appearance of β-Ti under high temperature at moderate pressure (see Fig. 3).

C. Above 10 GPa: ω-Ti, β-Ti, γ-Ti, and δ-Ti

Above 10 GPa, the following phases have been observed (see Fig. 4): ω-Ti, γ-Ti, δ-Ti, and β-Ti. We did not record any evidence of η-Ti around 80 GPa at high temperature, i.e., conditions where it has been reported [5]. All recorded diffraction peaks correspond to elements or compounds, which were placed in the pressure chamber (sample, pressure media, pressure gauges). Possible chemical reaction products were, therefore, below the detection limit (a few percent) of the XRD technique. The observed stability fields of the solid high-pressure phases of titanium are represented in Fig. 5 and are discussed below.

The XRD signals of ω-Ti and β-Ti differ only by a few additional diffraction lines for ω-Ti (see Fig. 3). During laser-heating in runs 6–8, high-temperature recrystallization led to a modification of the initial powder XRD pattern to a pattern of several single crystals (see also Ref. [20]). We considered that β-Ti and ω-Ti were present when at least one peak specific of ω-Ti [(001), (111), or (002)] was recorded in addition to the peaks which belong to both ω-Ti and β-Ti. Large coexistence temperature domains of ω-Ti and β-Ti were measured in run 6, which we interpret as a proof of temperature gradients within the sample. These domains were much narrower for the thinner sample used in run 7; we therefore used the temperature of disappearance of ω-Ti in run 7 to locate the ω-β phase boundary represented in Fig. 5. The measured volumes of ω-Ti and β-Ti near the phase boundary are close: $V_\beta - V_\omega \leqslant 1\%$ up to 100 GPa. This small volume difference is compatible with the small Clapeyron slope represented in Fig. 5. The low-temperature phases (ω-Ti, γ-Ti, or δ-Ti) reappeared after quench to 300 K.

ω-Ti transformed into γ-Ti between 115 and 120 GPa during the isothermal compression run in helium (run 3) and after laser-heating (run 7). This transition pressure is close to the ones reported in Refs. [3] and [4], both performed under nonhydrostatic pressurizing conditions and without laser-heating.

The stability field of δ-Ti has been reached in runs 7 and 8. It appeared above 135 GPa after heating, a pressure in good

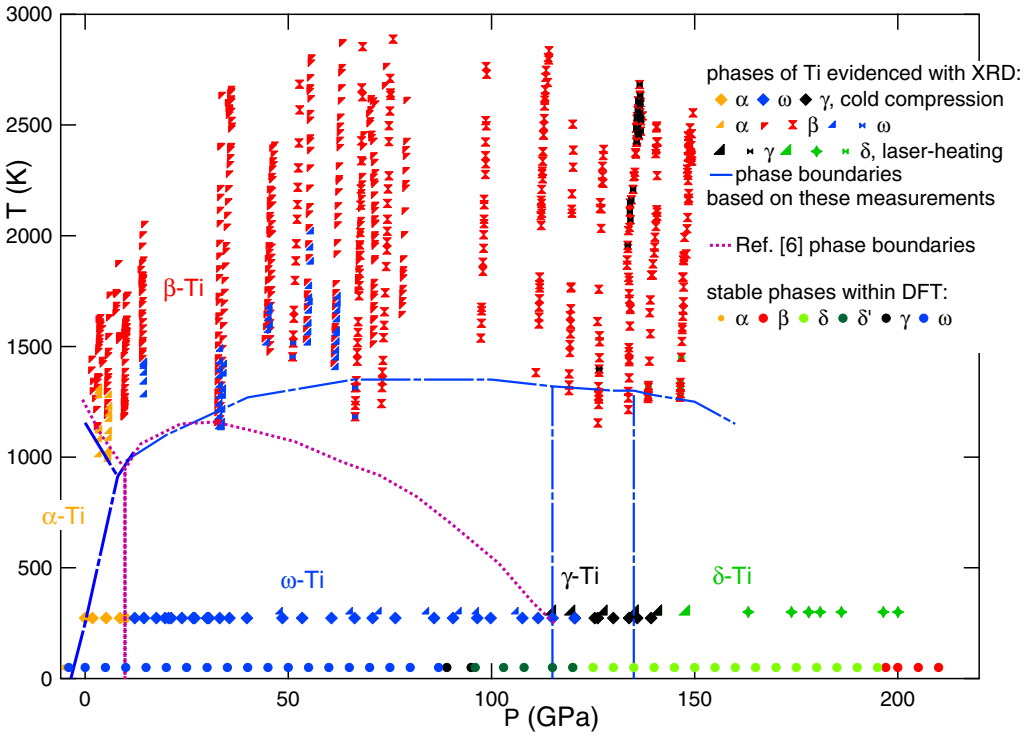

FIG. 5. (Color online) P-T conditions at which XRD data points have been recorded for solid titanium. The temperature has been measured by pyrometry. The pressure has been measured using the pressure gauges specified in Table I. The symbols' color and shape indicate, respectively, the phase of Ti and run number. The blue dashed lines are tentative phase boundaries based on the current data and literature low pressure studies [1]; they are compared with the boundaries proposed in Ref. [6]. The dots indicate the stable phases according to present DFT calculations (see Sec. III B).

agreement with the one reported in Ref. [4] (140–145 GPa) when the difference in pressure metrology is taken into account (Akahama *et al.* used a platinum pressure gauge which overestimates the pressure compared to our pressure gauge [19]). δ-Ti has been observed up to 200 GPa, the maximum pressure reached in this study, after laser-heating up to $\simeq$3000 K in run 8 (see Fig. 5). This suggests that δ-Ti is not a metastable phase synthesized as a result of nonhydrostatic stresses as suggested earlier [9,11,13,14]. The stability of δ-Ti is in line with present *ab initio* calculations as explained in Sec. III.

III. CALCULATED SEQUENCE OF PHASE TRANSITIONS AT HIGH PRESSURE

A. Summary of previous studies

The high-pressure phase transition sequence of Ti has been studied in the past decade in the framework of DFT using the generalized gradient approximation (GGA [26]) exchange correlation functional, with various conclusions summarized in Table II. Verma *et al.* [10] used the augmented plane wave (APW) with local orbital method and found the sequence ω-γ-β with transition pressures of 102 and 112 GPa. The structural parameters of the ω, γ, and δ phase were kept constant, meaning that the structures were not fully relaxed as a function of the volume. Kutepov *et al.* [9] used the all-electrons full-potential linear-augmented-plane-wave method (FLAPW) method and performed full geometry optimization. They found a ω-γ-δ-β sequence with transition pressures of 98, 106, and 136 GPa. Hao *et al.* [13] used the projector augmented wave (PAW) method with the VASP code and cell optimization. They found a sequence ω-γ-δ-β with transition pressures of 106, 135, and 161 GPa. Two years later, Hao *et al.* [12] performed similar calculations but including also the $3s$ and $3p$ semicore states as valence electrons. The δ phase was no longer stable and a ω-γ-β sequence has been obtained. Mei *et al.* [11] also used VASP but with denser k-point samplings. They reported a similar sequence, ω-γ-β, with

TABLE II. Calculated and measured phase transition pressures of titanium reported in the literature, compared with the present results. The GGA-PBE [26] exchange-correlation functional was used for all calculations. δ'-Ti is not reported because it is expected to become unstable above $\simeq$200 K (see Sec. III E).

	Phase transitions (GPa)			
Method and reference	$\omega \rightarrow \gamma$	$\gamma \rightarrow \delta$	$\delta \rightarrow \beta$	$\gamma \rightarrow \beta$
FLAPW (Kutepov *et al.*, 2003) [9]	98	106	136	–
APW-LO (Verma *et al.*, 2007) [10]	102	–	–	112
VASP (Hao *et al.*, 2008) [13]	106	135	161	
VASP (Hao *et al.*, 2010) [12]	117	–	–	162
VASP (Mei *et al.*, 2009) [11]	105	–	–	107
ABINIT LCP	95	–	–	106
ABINIT SCP	88	107	196	–
Exp., this work, up to 200 GPa	117	135	–	–
Exp., Ref. [3], up to 146 GPa	116	–	–	–
Exp., Ref. [4], up to 220 GPa	128	140	–	–

transition pressures of only 105 and 107 GPa. They stressed the effect of the fitting schemes (third-order Birch-Murnaghan or Vinet EoS) used to obtain pressure from the E-V data. To avoid this problem, they calculated the pressure directly via the diagonal stress components instead of using the value from the EoS.

All those studies obtain small enthalpy differences between the candidate high-pressure structures (in particular, less than 5 meV per atom between δ-Ti and β-Ti [11]). To be predictive, the calculations should, therefore, be carefully done with a fine plane wave basis set and a dense sampling of the Brillouin zone. The structures have to be fully relaxed and the pressure must be deduced from the computed stress tensor.

B. DFT methods

Present calculations were performed with the ABINIT package [27], using DFT with the GGA exchange-correlation functional of Perdew, Burke, and Ernzerhof [26] (PBE) as in previous studies. It has already been shown that GGA predicts more accurate lattice parameters of Ti than the local density approximation [28]. The PAW method [29] was adopted with a PAW atomic dataset involving 12 valence electrons ($3s^2$, $3p^6$, $4s^2$, $3d^2$). Two plane-wave basis sets with energy cutoff of 816 and 1088 eV were used (see discussion below). The precision reached was about 1 meV/atom.

The ω, γ, and the δ phases were fully relaxed and the pressure was converged up to 0.01 GPa with the diagonal stress components identical up to 6 digits to avoid nonhydrostatic conditions. For the k-point sampling of the Brillouin zone, we used the same values as Mei *et al.* [11]: $16 \times 16 \times 10$ for α-Ti, $25 \times 25 \times 25$ for β-Ti, $17 \times 17 \times 24$ for ω-Ti, $27 \times 27 \times 15$ for γ-Ti, and $25 \times 25 \times 15$ for δ-Ti.

We have studied the effect of the core radius of the atomic spheres on the calculations result. This radius should be sufficiently small to avoid overlapping of the spheres in the relevant pressure domain. Using ATOMPAW [30–32] code, we have generated two PAW atomic datasets: one with a radius $r_{\mathrm{PAW}} = 1.2$ Å, as in Refs. [11] and [12], called LCP (large core PAW) and one with $r_{\mathrm{PAW}} = 1.0$ Å, called SCP. To ensure the same accuracy for both PAW atomic datasets, we used a plane-wave energy cutoff of 816 and 1088 eV for LCP and SCP, respectively.

C. Effect of the PAW core radius

The relative enthalpies of titanium structures versus pressure above 80 GPa are presented in Fig. 6 for the two PAW atomic datasets.

With the SCP atomic dataset, we predict a stability domain for δ-Ti (Fig. 6, left panel). However, in the 80–120 GPa pressure range, the lattice parameters of the relaxed phase deviate from the experimental values for δ-Ti: $a/b \sim 1.69$ and $c/b \sim 1.54$ in present calculations compared to $a/b \sim 1.46$ and $c/b \sim 1.38$ in experiments, while the y values are similar, 0.31 compared to 0.30 (see Fig. 7). Therefore, this structure must be considered as a new phase and will be named hereafter δ'. We thus obtain a sequence ω-γ-δ'-δ-β with transition pressures of 88, 96, 120, and 196 GPa.

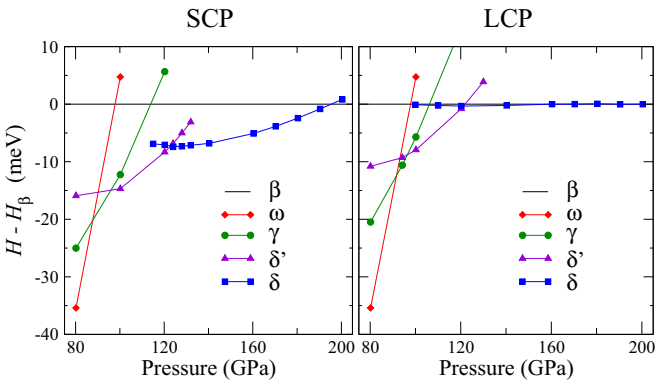

FIG. 6. (Color online) Calculated enthalpy differences of ω, γ, and δ phases with respect to the β phase as a function of pressure for two PAW atomic datasets: with a large radius (1.2 Å), LCP, on the right panel and with a small radius (1.0 Å), SCP, on the left panel, see text for more details.

With the LCP, the results differ significantly: the δ phase is no more stable, because the relaxation of this structure gives $a/b = c/b \approx \sqrt{2}$ and $y \approx 1/4$, corresponding to the β-Ti structure. However, starting with SCP parameters, the δ' phase can be relaxed and stabilized with a lower energy than γ and β between 97 and 120 GPa. If this phase is not taken into account, we find a ω-γ-β sequence, with transition pressures of 95 and 106 GPa (see Table II), in agreement with Ref. [11] study, which was performed with similar parameters.

The enthalpies of the open orthorhombic structures, γ, δ, and δ' are lower using the SCP than with the LCP atomic dataset (Fig. 6). This can be attributed to an overlapping

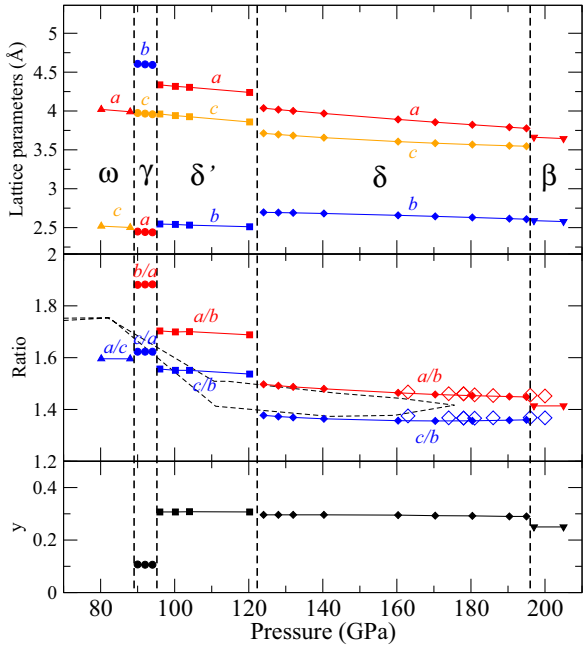

FIG. 7. (Color online) Calculated pressure dependence of the lattice parameters, ratios, and internal parameter y of the ω, γ, δ', δ, and β phases, for the SCP atomic dataset ($r_{\mathrm{PAW}} = 1.0$ Å). The dashed line corresponds to Kutepov *et al.* [9] results for the δ phase. The open diamonds correspond to the present experimental ratios for the δ phase.

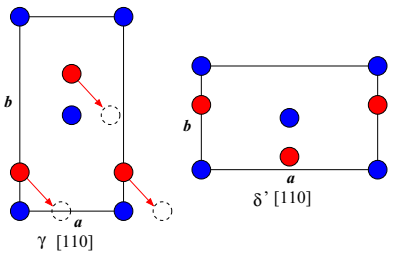

FIG. 8. (Color online) Schematic representation of a possible γ to δ' transition in titanium.

between the atomic spheres of LCP. At 130 GPa, the first nearest-neighbor distance is 2.15 Å and 2.36 Å for the δ and the β phase, respectively. Therefore, with $r_{\mathrm{PAW}} = 1.2$ Å (LCP), atomic spheres overlap in δ-Ti and not in β-Ti, which artificially favors β-Ti. As a result, the enthalpy of δ-Ti is overestimated and this structure spontaneously transforms into β-Ti when it is relaxed. With SCP, there is no overlapping between atomic spheres in δ-Ti below $\simeq$280 GPa.

D. Comparison with all-electron calculations

The current prediction of the stability of δ-Ti agrees with the all electrons calculations results of Kutepov *et al.* [9], which do not suffer from the choice of the core radius r_{PAW}. The lattice parameters also agree: below 100 GPa (out of the stability field of δ-Ti), we find lattice parameters ratios a/b and c/b around 1.75 for δ-Ti, similar to the 80 GPa value in Ref. [9]. Between 120 and 160 GPa, the a/b and c/b ratios of δ-Ti also agree (see Fig. 7); they show a weak pressure dependence and do not evolve toward the value of $\sqrt{2}$ corresponding to β-Ti. Interestingly, Kutepov *et al.* [9] could not converge their calculations between 80 and 110 GPa, the approximate pressure range where we predict δ'-Ti to be stable.

Due to some oscillations in their enthalpy curve that they attributed to their poor Brillouin-zone sampling, Kutepov *et al.* obtained a δ-β transition pressure of 135 GPa. In present calculations the denser sampling of the Brillouin zone may explain the larger stability domain for the δ phase.

The new δ' structure can be seen as intermediate between the γ and the δ structures. In fact, the lattice parameters a and b seems to be swapped with each other in γ-Ti and δ'-Ti; see Fig. 7. This can easily be done by a shuffle of one of the atoms plane along the $[1\bar{1}0]$ direction; see Fig. 8. It is remarkable that this shuffle is similar to the one involved in the Burger's mechanism [33], which transforms a hcp into a bcc structure.

E. Comparison with experimental data

The current calculations predict that the α-ω transformation takes place at -4.6 GPa, in accordance with recent *ab initio* results [9,11] and with the experimental data (see Sec. II B). At higher pressure, γ-Ti and δ-Ti are correctly predicted to be stable, with lattice parameters similar to the experimental ones (see Fig. 7). However, some divergences between our calculations performed at 0 K and the experiments at room or higher temperature remain.

The δ' structure is not observed experimentally. A possible explanation is that the entropy from thermal population of phonon states stabilizes the δ and γ structures over δ' at room temperature. Indeed, the enthalpy difference between δ'-Ti and δ-Ti is smaller than 5 meV/atom (Fig. 6) and entropy terms, even small, can have a strong impact on the stability field of each phase.

In order to quantitatively test this hypothesis, we have performed *ab initio* molecular dynamics (AIMD) calculations on δ and δ' phases at 110 GPa, at 300 and 1000 K. We used supercells of 96 atoms ($2 \times 4 \times 3$) and a $2 \times 4 \times 2$ k-point mesh for the sampling of the Brillouin zone. AIMD simulations were run for about 2 ps. To extract the vibrational frequencies from the AIMD simulations we used the method recently developed by Hellman *et al.* [34,35]. The calculated phonon spectra are presented in Fig. 9 for the δ and δ' phase. They are similar and exhibit a strong softening of one optical branch between 300 and 1000 K (see the red arrows and the thick red lines in Fig. 9), suggesting that these structures are unstable at high temperature.

Using the calculated phonon density of states, the Gibbs free energy $G(P,T)$ can be evaluated at 110 GPa by adding the vibrational entropy contribution to the enthalpy. The results are shown in the right panel of Fig. 9. The vibrational entropy favors δ-Ti over δ'-Ti above 200 K: this possibly explains why δ'-Ti has not been observed in experiments at 300 K.

The current theoretical ω-γ and γ-δ phase transition pressures are lower than experimental ones by around 20 GPa. This

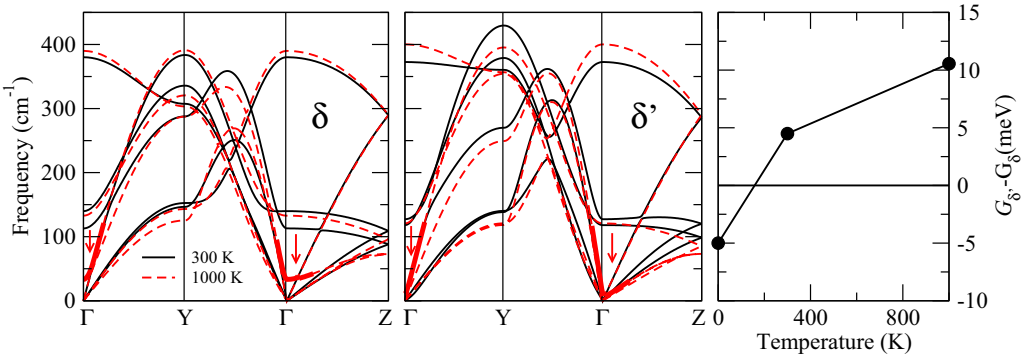

FIG. 9. (Color online) Phonon spectra of δ (left panel) and δ' (center panel) titanium at 300 K (black lines) and 1000 K (red dashed lines) at 110 GPa. The red thick line is the low-frequency optical branch around the Γ point calculated at 1000 K. The right panel shows the calculated Gibbs free-energy difference between δ' and δ phases as a function of temperature at 110 GPa.

may be explained by metastability effect in the experiments, although it is less likely when the laser-heating technique is used. The volumes (and not the pressures) of phase transitions should be compared; however, the calculated EoS of Ti is very close to the experimental one (see Sec. IV A), even if lower, so that the EoS difference explains only a small part of the transition pressure difference. The present calculations predict a δ-β phase transition at 196 GPa, higher than all previous theoretical studies (see Table II). This reduces the gap between theoretical predictions and experimental observations (β-Ti is not observed at 300 K up to 220 GPa [4]). It should be noted that the enthalpy curves of δ-Ti and β-Ti versus P have a low angle (Fig. 6, SCP): a small error in the enthalpy of one phase would result in a large error in the estimated phase transition pressure. As a consequence, the estimated δ-β transition pressure is uncertain but the trend in Fig. 6 is clear: pressure increase favors β-Ti. It is thus reasonable to expect that β-Ti will eventually be observed at 300 K in experiments carried out above 220 GPa.

IV. EQUATIONS OF STATE

A. Ambient temperature equations of state

The P-V points measured in runs 1–3 and 8 are plotted in Fig. 10 (see Table IV). These points, as well as the calculated ones (see Sec. III B), have been fitted with a Rydberg-Vinet EoS formulation [36]; the fit parameters are listed in Table III. Experimental and theoretical compression curves for ω-Ti are very close to each other, with a difference of less than 1.3% in volume [see Fig. 10 (b)], which is in part due to the thermal expansion between 0 and 300 K. This good agreement, which appears also in the EoS parameters listed in Table III, validates the functional and approximations used in the calculations. The experimental bulk modulus K_0 for ω-Ti is lower than measured in earlier studies (138 GPa [2], 142 GPa [3], and 123 GPa [4]), which is expected if the previous measurements have been affected by nonhydrostatic stresses—which lead to an overestimate of volume, and therefore bulk modulus, under pressure [16]. However, the P-V points measured in nonhydrostatic compression [4] for ω-Ti, γ-Ti, and δ-Ti are surprisingly close to the current ones, which can be due to a compensation of errors. A model compression curve based on shock compression data [6] is slightly softer than the current one for ω-Ti. The bulk modulus of γ-Ti estimated using P-V points between 125 and 140 GPa is surprisingly low and significantly differs from the calculated one (Table III), which could be related to the narrow stability range of this phase.

The c/a ratio in ω-Ti exhibits a smooth variation (Fig. 10 and Table IV), an observation that differs from a previous report [5], where a discontinuous change of this ratio was interpreted as an evidence of the formation of a β'-Ti bcc phase. c/a decreases above 100 GPa and an extrapolation of this trend would cross the value of $\sqrt{3}/\sqrt{8} = 0.612$, for which the ω phase is identical to a bcc phase, around 150 GPa. This softening, also seen in the DFT calculations, can be seen as a precursor of the phase transformation of ω-Ti to a higher-pressure phase.

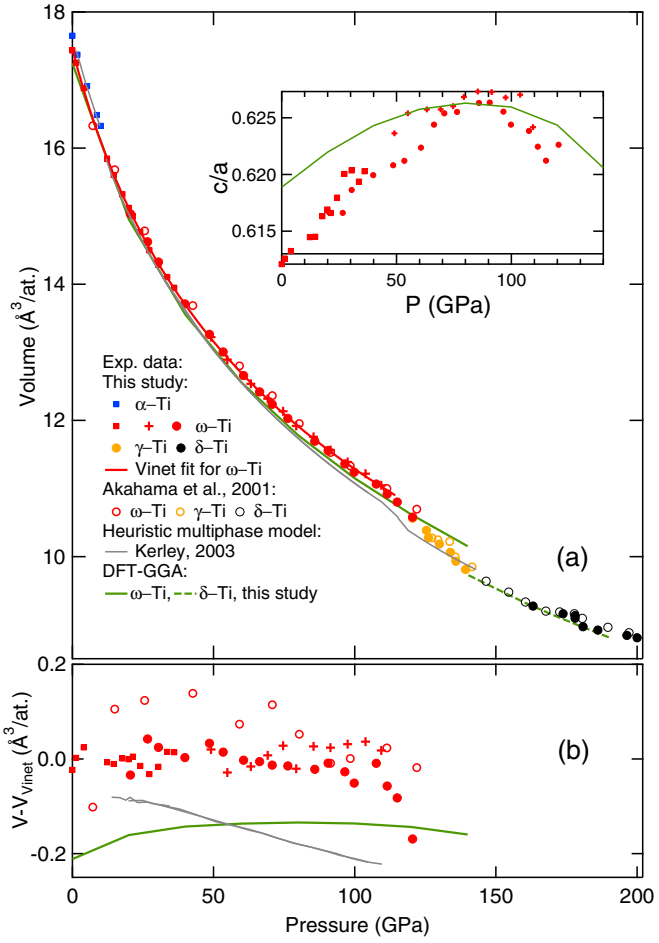

FIG. 10. (Color online) (a) P-V points measured at 300 K in helium pressure medium for α-Ti, ω-Ti, γ-Ti, and in KCl pressure medium for δ-Ti. Different symbols correspond to different experimental runs. The compression curve of ω-Ti has been fitted with a Rydberg-Vinet EoS (see text). The present DFT-GGA calculations, Ref. [4] measurements, and Ref. [6] model are also plotted. Inset: evolution of the c/a ratio in ω-Ti with pressure; same symbols as in the main graph. (b) Difference between measured and fit volume for ω-Ti.

B. Equation of state of β-Ti under high temperature

The EoS of β-Ti has been measured in run 6. Pressure and temperature metrology are critical questions during laser-heating, which induces temperature and pressure inhomogeneities in the pressure chamber [37]. We have followed the same method as in Ref. [20]: a thin ($\simeq$2 μm) disk of MgO was placed on the surface of the Ti sample and used as an XRD pressure gauge. Its temperature and pressure P_{MgO} were assumed to be equal to the surface temperature and pressure of the laser-heated sample. P_{MgO} was deduced from its measured volume and equation of state [18]. During a heating series, P_{MgO} was observed to increase by 3 GPa at most, due to thermal pressure [37]. The lattice parameter measured for β-Ti during six heating series is plotted in Fig. 11, and the corresponding data are given in Supplemental Material [38]. As expected, its thermal expansion decreases with increasing pressure.

TABLE III. Rydberg-Vinet EoS [36] parameters for α-Ti and ω-Ti obtained in this study by a fit of experimental data at 300 K and DFT calculations at 0 K (see Sec. III B). Bold number has been fixed during the fit. The error bars on the last two digits correspond to 95 percent confidence interval. The volume discontinuity at the α-ω phase transition at 0.6 GPa, is -1.1%. The bulk moduli measured and calculated in the stability domain of γ-Ti are also given.

Phase	Method	V_0 (Å^3/at), K_0 (GPa), K_0'
α-Ti	Exp.	17.652(20), 110.4(2.7), **4**
ω-Ti	Exp.	17.46(10), 106.9(6.0), 3.68(20)
ω-Ti	ABINIT SCP	17.246, 113.3, 3.40
γ-Ti	Exp.	$K \approx 300$ GPa at 130 GPa
γ-Ti	ABINIT SCP	$K \approx 450$ GPa at 130 GPa

We have reproduced the thermal expansion measured at high and ambient pressure [39] with a quasiharmonic model based on a single Debye temperature θ and Grüneisen parameter γ: in this model, the free-energy F expresses as $F(V,T) = F_0(V) + F_i(V,T)$, where $F_0(V)$ is the static lattice component, $F_i(V,T)$ represents the contribution from ionic motion. Its volume derivative, e.g., the thermal pressure, is approximated by the following expression [20]:

$$P_i(V,T) = 9k_B T\left(\frac{B}{V} + A\right)\left[\frac{\theta}{8T} + \frac{1}{3}D\left(\frac{\theta}{T}\right)\right], \quad (1)$$

where $D(\theta/T)$ is the Debye function and θ is defined as

$$\theta(V) = \theta^{(0)}\left(\frac{V}{V_{\text{ref}}}\right)^{-B}\exp[A(V_{\text{ref}} - V)]. \quad (2)$$

This corresponds to the following expression for the Grüneisen parameter:

$$\gamma = A \times V + B. \quad (3)$$

The cold pressure $P_0(V) = -dF_0/dV$ is expressed with a Rydberg-Vinet EoS [36].

The value of θ_0 has been taken from the literature: 317 K [6]. The best parameters for $P_0(V)$ EoS were $V_0 = 17.8$ Å^3, $K_0 = 96$ GPa, $K_0' = 3.1$, in correct agreement with earlier estimates for β-Ti [6] and also close to the EoS parameters for ω-Ti.

TABLE IV. Lattice parameters (a, b, and c) of α-Ti, ω-Ti, γ-Ti, and δ-Ti at 300 K for three runs (see Table I). P is in GPa (determined using the following pressure markers: ruby [18] in runs 1 and 2, W [18] in run 3, and KCl [21] in run 8), and lattice parameters are in Å. The data are listed in the order they have been taken. The volume per formula unit plotted on Fig. 10 are $V_\alpha = a_\alpha^2 \times c_\alpha\sqrt{3}/4$, $V_\omega = a_\omega^2 \times c_\omega/2\sqrt{3}$, and $V_{\gamma,\delta} = a_{\gamma,\delta} \times b_{\gamma,\delta} \times c_{\gamma,\delta}/4$.

Run	P	a_α	c_α	a_ω	c_ω	Run	P	a_ω	c_ω	a_γ	b_γ	c_γ	a_δ	b_δ	c_δ
1	1.8	2.935	4.659			3	20.5	4.387	2.706						
	5.2	2.908	4.618				26.6	4.347	2.681						
	8.64	2.885	4.576				30.5	4.313	2.668						
	10	2.875	4.561				39.8	4.247	2.633						
	12.3			4.470	2.747		48.6	4.199	2.607						
	14.6			4.447	2.733		53.4	4.170	2.591						
	17.7			4.416	2.722		60.6	4.130	2.571						
	19.9			4.396	2.712		66.3	4.010	2.560						
	21.4			4.384	2.703		70.8	4.077	2.550						
	24.1			4.358	2.693		76.3	4.054	2.536						
	27.3			4.327	2.683		85.9	4.014	2.514						
	30.4			4.305	2.671		90.6	3.999	2.504						
	36.1			4.271	2.649		96.5	3.977	2.488						
	33.6			4.289	2.657		99.8	3.966	2.476						
	4			4.569	2.802		108	3.946	2.462						
	1.29			4.604	2.820		111	3.931	2.447						
	0			4.621	2.828		115	3.920	2.435						
2	49.1			4.174	2.603		121	3.890	2.422	2.390	4.51	3.920			
	54.9			4.135	2.586		125			2.385	4.466	3.900			
	63.2			4.096	2.563		126			2.377	4.455	3.882			
	69.2			4.072	2.548		130			2.372	4.435	3.872			
	74.6			4.051	2.536		134			2.367	4.410	3.856			
	79.3			4.025	2.523		136			2.360	4.395	3.830			
	85.4			4.006	2.513		139			2.354	4.375	3.810			
	91.4			3.984	2.499	8	163						3.873	2.639	3.629
	97.5			3.965	2.485		174						3.852	2.637	3.607
	103.8			3.944	2.473		178						3.8497	2.635	3.602
	109.4			3.93	2.453		178						3.843	2.632	3.597
							181						3.819	2.622	3.583
							186						3.806	2.618	3.581
							196						3.796	2.609	3.571
							200						3.787	2.608	3.567

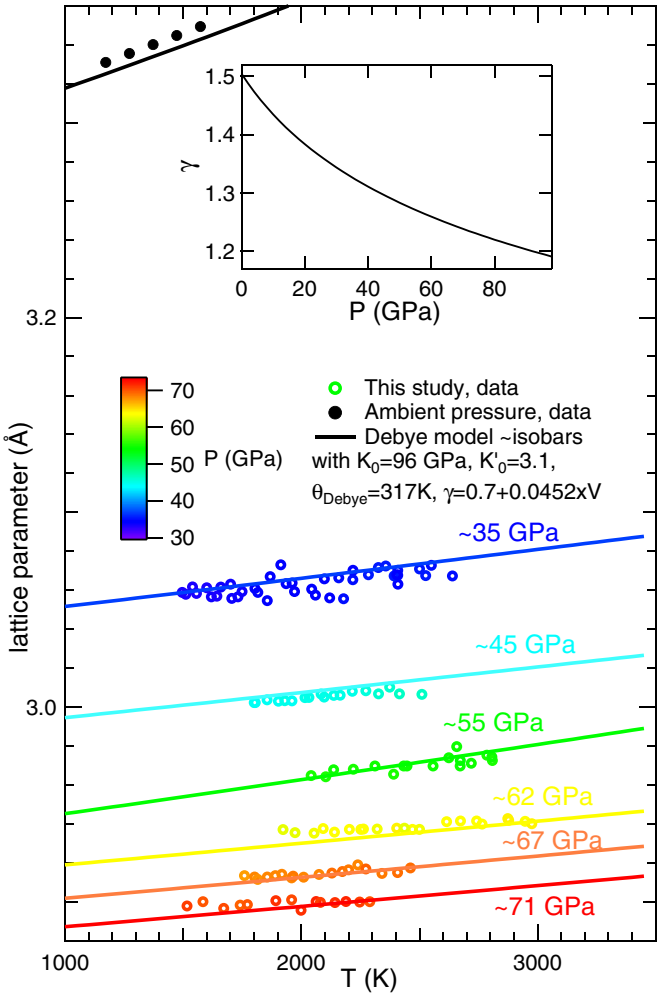

FIG. 11. (Color online) Lattice parameter of β-Ti vs temperature. The data and the model (see text) are plotted as circles and lines, respectively. Inset: Grüneisen parameter γ vs pressure at 300 K, calculated using Eq. (3) with $A = 0.0452\,\text{Å}^{-3}$ and $B = 0.7$.

We propose the following parameters: $B = 0.7$, $A = 0.0452\,\text{Å}^{-3}$ for Eq. (3) to reproduce the measured thermal expansion. This set of parameters has been used to generate the continuous lines plotted on Fig. 11 (the pressure follows P_{MgO}). We have also compared the EoS for β-Ti proposed by Kerley [6] and the current data. The difference between the measured pressure and the calculated pressure at the same volume of β-Ti is zero in average, with no trend with pressure and temperature, which means that EoS for β-Ti in Ref. [6] correctly reproduces the measurements.

V. CONCLUSION

The sequence of phase transformations and equation of state of Ti have been measured under quasihydrostatic conditions (in helium pressure transmitting medium) up to 139 GPa at ambient temperature and up to 15 GPa between 300 and 737 K. The measured conditions of the α-Ti/ω-Ti transition support the theoretical finding that ω-Ti is stable at ambient pressure and 0 K. At 300 K, we confirm the sequence measured earlier, under nonhydrostatic pressurizing conditions: $\alpha \rightarrow \omega \rightarrow \gamma \rightarrow \delta$, with similar transition pressures. Laser-heating measurements show that β-Ti is stable above $\simeq$1300 K in the scanned pressure range (0–200 GPa) and we have measured its high pressure-high temperature equation of state below 75 GPa. We did not reach the predicted stability field of β-Ti at 300 K up to 200 GPa, even after laser-heating. The present *ab initio* calculations correctly predict the stability of γ-Ti and δ-Ti. Earlier studies [10–12] did not obtain these phases because the crystalline cell parameters were not relaxed and/or the core radius of the pseudopotential for Ti was too high to describe correctly these high-pressure phases. The example of titanium thus illustrates the danger of using parameters of density-functional theory established for ambient conditions as also granted under high compression, and to use them for crystal structure predictions. The predicted transition pressures are $\simeq$20 GPa lower than the corresponding measured transition pressures. It is possible that a phase transition toward the bcc β phase, predicted at 196 GPa, will be observed above 220 GPa, the highest pressure reached in experiments [4]. A new structure, called δ', is predicted to be stable between 96 and 120 GPa at 0 K, but the calculation of vibrational properties indicate that this structure becomes unstable above $\simeq$200 K.

ACKNOWLEDGMENTS

We acknowledge the European Synchrotron Radiation Facility for the provision of synchrotron radiation under proposals HS-3739 and HC-839. We thank M. Hanfland and C. Pépin for experimental help and P. Loubeyre for his comments on the manuscript.

[1] E. Y. Tonkov and E. G. Ponyatovsky, *Phase Transformations of Elements under High Pressure* (CRC Press, Boca Raton, 2004).
[2] D. Errandonea, Y. Meng, M. Somayazulu, and D. Hausermann, Physica B **355**, 116 (2005).
[3] Y. K. Vohra and P. T. Spencer, Phys. Rev. Lett. **86**, 3068 (2001).
[4] Y. Akahama, H. Kawamura, and T. Le Bihan, Phys. Rev. Lett. **87**, 275503 (2001).
[5] R. Ahuja, L. Dubrovinsky, N. Dubrovinskaia, J. M. Osorio Guillen, M. Mattesini, B. Johansson, and T. L. Bihan, Phys. Rev. B **69**, 184102 (2004).
[6] G. I. Kerley, *Equations of State for Titanium and Ti6A14V Alloy*, Tech. Rep. 3785, Sandia National Laboratories (U.S. Department of Commerce, Springfield, VA, 2003).
[7] R. Ahuja, J. M. Wills, B. Johansson, and O. Eriksson, Phys. Rev. B **48**, 16269 (1993).
[8] K. D. Joshi, G. Jyoti, S. C. Gupta, and S. K. Sikka, Phys. Rev. B **65**, 052106 (2002).
[9] A. L. Kutepov and S. G. Kutepova, Phys. Rev. B **67**, 132102 (2003).
[10] A. K. Verma, P. Modak, R. S. Rao, B. K. Godwal, and R. Jeanloz, Phys. Rev. B **75**, 014109 (2007).

[11] Z.-G. Mei, S.-L. Shang, Y. Wang, and Z.-K. Liu, Phys. Rev. B **80**, 104116 (2009).
[12] Y.-J. Hao, J. Zhu, L. Zhang, J. Qu, and H. Ren, Solid State Sci. **12**, 1473 (2010).
[13] Y.-J. Hao, L. Zhang, X.-R. Chen, Y.-H. Li, and H.-L. He, Solid State Comm. **146**, 105 (2008).
[14] C.-E. Hu, Z.-Y. Zeng, L. Zhang, X.-R. Chen, L.-C. Cai, and D. Alfe, J. Appl. Phys. **107**, 093509 (2010).
[15] S. Pecker, S. Eliezer, D. Fisher, Z. Henis, and Z. Zinamon, J. Appl. Phys. **98**, 043516 (2005).
[16] A. Dewaele and P. Loubeyre, High Press. Res. **27**, 419 (2007).
[17] K. Takemura, H. Yamawaki, H. Fujihisa, and T. Kikegawa, Phys. Rev. B **65**, 132107 (2002).
[18] P. I. Dorogokupets and A. R. Oganov, Phys. Rev. B **75**, 024115 (2007).
[19] A. Dewaele, P. Loubeyre, and M. Mezouar, Phys. Rev. B **70**, 094112 (2004).
[20] A. Lazicki, A. Dewaele, P. Loubeyre, and M. Mezouar, Phys. Rev. B **86**, 174118 (2012).
[21] A. Dewaele, A. B. Belonoshko, G. Garbarino, F. Occelli, P. Bouvier, M. Hanfland, and M. Mezouar, Phys. Rev. B **85**, 214105 (2012).
[22] M. Mezouar *et al.*, J. Synchtrotron Rad. **12**, 659 (2005).
[23] L. Benedetti and P. Loubeyre, High Press. Res. **24**, 423 (2004).
[24] J. Zhang, Y. Zhao, R. S. Hixson, G. T. GrayIII, L. Wang, W. Utsumi, S. Hiroyuki, and H. Takanori, J. Phys. Chem. Solids **69**, 2559 (2008).
[25] Y. S. Ponosov, S. V. Streltsov, and K. Syassen, High Press. Res. **32**, 138 (2012).
[26] J. P. Perdew, K. Burke, and M. Ernzerhof, Phys. Rev. Lett **77**, 3865 (1996).
[27] X. Gonze, Comput. Mater. Sci. **25**, 478 (2002).
[28] G. Jomard, L. Magaud, and A. Pasturel, Philos. Mag. B **77**, 67 (1998).
[29] P. E. Blöchl, Phys. Rev. B **50**, 17953 (1994).
[30] N. Holzwarth, A. Tackett, and G. Matthews, Comput. Phys. Commun. **135**, 329 (2001).
[31] A. Dewaele, M. Torrent, P. Loubeyre, and M. Mezouar, Phys. Rev. B **78**, 104102 (2008).
[32] ATOMPAW is a general license public code developed at Wake Forest University. Some of its capabilities have been developed at the Commissariat à l'Energie Atomique http://pwpaw.wfu.edu.
[33] W. G. Burgers, Physica **1**, 561 (1934).
[34] O. Hellman, I. A. Abrikosov, and S. I. Simak, Phys. Rev. B **84**, 180301(R) (2011).
[35] O. Hellman, P. Steneteg, I. A. Abrikosov, and S. I. Simak, Phys. Rev. B **87**, 104111 (2013).
[36] P. Vinet, J. Ferrante, J. H. Rose, and J. R. Smith, J. Geophys. Res. **92**, 9319 (1987).
[37] A. Dewaele, G. Fiquet, and P. Gillet, Review Sci. Intrum. **69**, 2421 (1998).
[38] See Supplemental Material at http://link.aps.org/supplemental/10.1103/PhysRevB.91.134108 for the data plotted on Fig. 11 (2015).
[39] O. N. Senkov, B. C. Chakoumakos, J. J. Jonas, and F. H. Froes, Mat. Res. Bull. **36**, 1431 (2001).